Dalton Transactions

ROYAL SOCIETY OF CHEMISTRY

PAPER

View Article Online
View Journal | View Issue

Cite this: *Dalton Trans.*, 2025, **54**, 16163

Oxidative addition chemistry of bis(4,5-dimethoxybenzo)-1,2,5,6-tetrathiocin with cyclopentadienyl metal carbonyl complexes and the mechanochemical transformation of CpCo(dmobdt) to $[CpCo(dmobdt)]_2$

Mary El Rayes,[a] Daniel J. Cutler,[a,f] Lara K. Watanabe,[a,b] Nadia T. Stephaniuk,[a,c] John J. Hayward,[a] Mike D'Agostino,[d] Charles L. B. Macdonald,[a,e] Melanie Pilkington[d] and Jeremy M. Rawson*[a]

Received 17th July 2025,
Accepted 18th August 2025

DOI: 10.1039/d5dt01691f

rsc.li/dalton

The oxidative addition of tetramethoxy-1,2,5,6-dibenzotetrathiocin (**1**) to $CpCo(CO)_2$, $[CpFe(CO)_2]_2$, $[CpMo(CO)_3]_2$ and $CpV(CO)_4$ in toluene under microwave irradiation (150 °C, 30 min) afforded the complexes CpCo(dmobdt) (**2**), $[Cp_2Fe_2(dmobt)(CO)_2]$ (**3**), $[Cp_2Mo_2(dmobdt)_2]$ (**4**) and $[(Cp)_2V_2(dmobdt)_2]$ (**5**) [dmobdt = 4,5-dimethoxybenzene-1,2-dithiolate dianion, $(MeO)_2C_6H_2S_2^{2-}$]. Vacuum sublimation of **2** afforded dark blue crystals of the monomeric 16e$^-$ complex, CpCo(dmobdt) (**2a**), whereas recrystallisation from CH_2Cl_2 afforded dark blue crystals of the dimeric 18e$^-$ polymorph, $[CpCo(dmodt)]_2$ (**2b**). The structures of **2a**, **2b**, **3**, **4** and **5** were determined by X-ray diffraction. DSC studies on **2a** and **2b** indicated distinct melting points (206 and 216 °C respectively) and VT-PXRD revealed no thermally-induced phase change between **2a** and **2b**. Conversely, mechanochemical grinding of **2a** revealed an irreversible phase transition to **2b**.

Introduction

The term "dithiolene" was introduced to describe the redox-active "dithiolene" (dt) ligand system,[1] in which the ligand can variously adopt one of the following redox states: the dithiolate dianion, dt^{2-}, the semi-1,2-dithione $dt^{\bullet-}$ and neutral dithione, dt (Scheme 1). Common dithiolene ligands include mnt^{2-}, $tdas^{2-}$, tfd^{2-} and $dmit^{2-}$ in their dithiolate forms (Scheme 2) and their metal complexes have been explored for materials properties.[2] Applications of such complexes range from non-linear optics,[2,3] sensitisers in dye sensitised solar cells (DSSCs),[4] conducting[5,6] and magnetic materials[7,8] through to catalysis[9] and models for metalloenzymes.[10]

The ability to tune the redox properties of the dithiolene ligand is important for such applications and dithiolate ligands with both electron-withdrawing cyano groups, such as $dcbdt^{2-}$ and $cbdt^{2-}$ as well as π-electron donating groups such as $dmobdt^{2-}$ are known (Scheme 2).[11,12] Traditionally metal dithiolates are prepared *via* three synthetic routes: (i) salt metathesis, whereby s-block metal dithiolates and d-block metal salts undergo ligand exchange to form d-block dithiolates; (ii) condensation of dithiols with d-metal oxo, alkoxo and amido precursors and (iii) the oxidative addition of dithietes to low valent transition metals.[13] Benzene dithiolate (bdt^{2-}) and its derivatives are attractive ligands due to the ability to tune both the steric and electronic properties of the dithiolene ligand through judicious choice of electron-donat-

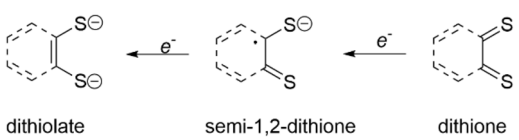

Scheme 1 Redox states of the dithiolene ligand.

[a]*Department of Chemistry and Biochemistry, University of Windsor, 401 Sunset Avenue, Windsor, Ontario N9B 3P4, Canada. E-mail: jmrawson@uwindsor.ca*
[b]*Department of Chemistry, University of Guelph, 50 Stone Road, Guelph, Ontario, N1G 2 W1, Canada*
[c]*Department of Chemistry, Kings College London, Britannia House, 7 Trinity Street, London, SE1 1DB, UK*
[d]*Department of Chemistry, Brock University, 1812 Sir Isaac Brock Way, St Catharines, Ontario, L2S 3A1, Canada*
[e]*Department of Chemistry, Dalhousie University, 6243 Alumni Crescent, PO Box 15000 Halifax, Nova Scotia, B3H 4R2, Canada*
[f]*Departament de Química Inorgànica i Orgànica, Universitat de Barcelona, Diagonal 645, 08028 Barcelona, Spain*

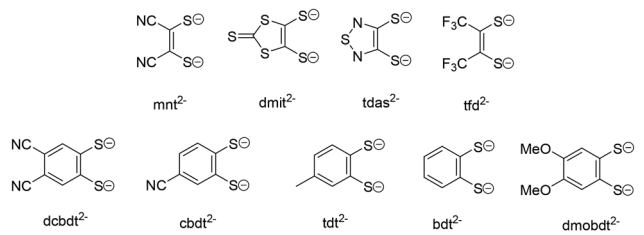

Scheme 2 Select dithiolate ligands.

ing, electron-withdrawing and/or sterically demanding groups. Yet benzene and toluene dithiolate ligands (bdt^{2-} and tdt^{2-}, Scheme 2) dominate this family with over 53% of benzene dithiolate derivatives in the CSD (release 5.46, Nov 2024) comprising bdt^{2-} or tdt^{2-}. This is most likely due to the commercial availability of benzene and toluene dithiols.[14,15] Synthetic route (iii) has been limited because of the small number of dithiete precursors, $R_2C_2S_2$ (R = CF_3, CO_2Me), with benzodithiete reportedly unstable above 180 K.[13,15] Previously, our group has described the oxidative addition of the 8-membered 1,2,5,6-tetrathiocin (**1**) to zero valent group 10 transition metal complexes such as $Ni(COD)_2$, M_2dba_3 (M = Pd, Pt) or $M(PR_3)_n$ as an efficient route to group 10 metal dithiolate complexes (Scheme 3).[16–19] This approach was recently extended to oxidative addition to the cobalt(I) complex, $CpCo(CO)_2$, generating CpCo(L) where L is the dithiolate derivative of benzo-15-crown-5 or benzo-18-crown-6.[12] To explore the generality of this reaction, we have now explored the microwave-assisted oxidative addition reaction of tetra-methoxy-dibenzotetrathiocin (**1**) to a range of early/mid/late 3d/4d transition metal ions of composition $CpM(CO)_n$ (M = V, Fe, Co and Mo), affording $[CpM(dmobdt)]_n$ (**2a** n = 1 M = Co; **2b** n = 2, M = Co; **4**, n = 2, M = V; **5** n = 2, M = Mo), and $Cp_2Fe_2(CO)_2$(dmobdt) (**3**) (Scheme 3). Within this series of complexes, the dithiolate adopts a chelating coordination mode but either one or both S atoms show the ability to also adopt a μ_2 bridging mode to satisfy the stereo-electronic demands of the metal centre. In particular, the solid-state conversion between **2a** and **2b** is explored and contrasted to previous studies on the closely related CpCo(bdt)/$[CpCo(bdt)]_2$ system.[20,21]

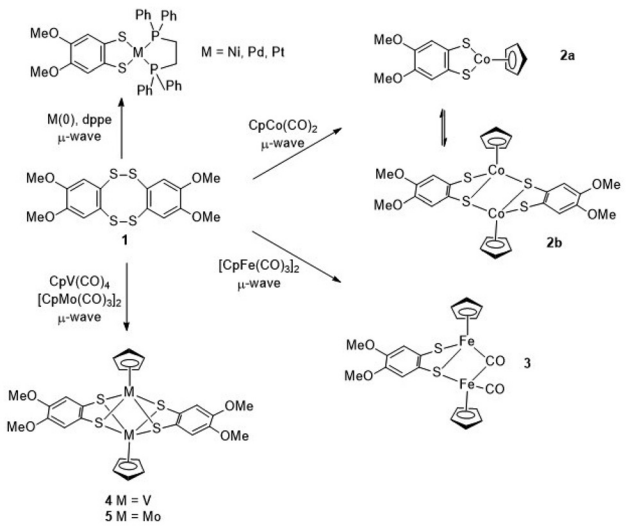

Scheme 3 Microwave-assisted oxidative addition reactions of tetrathiocin **1** with low valent metals afford dithiolate complexes.

Results and discussion

Synthetic procedures

Bis(4,5-dimethoxybenzo)-1,2,5,6-tetrathiocin, **1**, was prepared according to the previously described literature procedure.[22,23] The metal-dithiolate complexes, **2–5**, were all prepared by oxidative addition of the tetrathiocin **1** to the M(I) complexes $CpM(CO)_n$ in sealed containers using microwave irradiation.

Reaction of tetrathiocin **1** with cyclopentadienylcobalt dicarbonyl in toluene under microwave irradiation (150 °C, 30 min) formed an intense deep blue suspension. Extraction with chloroform and drying *in vacuo* afforded a dark blue solid from which dark blue crystals of the monomeric complex CpCo(dmobdt) (**2a**) were grown by vacuum sublimation onto a cold-finger (+175 to −3 °C). On the other hand, recrystallisation from dichloromethane selectively affords dark blue crystals of the dimeric complex, $[CpCo(dmodt)]_2$ (**2b**).

The reaction of tetrathiocin **1** with an excess of cyclopentadienyl iron dicarbonyl dimer, $[CpFe(CO)_2]_2$, under microwave irradiation (150 °C, 30 min) formed a brown/black suspension. Recrystallisation of the solid from chloroform afforded orange crystals of the dimeric iron dithiolate complex, $[Cp_2Fe_2(CO)_2(dmobdt)]$ (**3**). In an analogous fashion, reaction of **1** with an excess of $[CpMo(CO)_3]_2$ or $CpV(CO)_4$ afforded the dimeric bis-dithiolate metal complexes [CpMo(dmobdt)]$_2$ (**4**) and $[CpV(dmobdt)]_2$ (**5**).

Crystallographic details

Dark blue crystals of **2a** were formed *via* vacuum sublimation and were found to crystallize in the orthorhombic space group *Pbca* with one molecule per asymmetric unit. The structure of **2a** (Fig. 1) is a two-legged piano stool in which the Co atom is located just 0.044 Å from the C_6S_2Co mean plane, with a fold angle between CoS_2 and C_2S_2 planes of just 3.23°. The Co–S bond lengths fall in the range of 2.111(2)–2.128(2) Å. The C–S bond lengths are in the range of 1.726(6)–1.733(6) Å, typical of a dithiolate dianion. The Cp ring plane is essentially perpendicular to the C_2S_2 plane, at 85.03°. The Cp-centroid to Co distances of 1.657 Å is comparable with those of other 16e^- cyclopentadienyl cobalt(III) benzenedithiolate structures (1.640–1.656 Å).[21,24–27]

Crystals of **2b** were grown by slow diffusion of hexane into a saturated CH_2Cl_2 solution of **2**. It crystallizes in the monoclinic space group $P2_1/c$ with half a molecule in the asymmetric unit. The structure of the 18e^- dimer adopts a three-legged piano stool geometry at the Co(III) centre with an η^5-coordinate Cp ring and three sulfur atoms, comprising S1 and S2 from a chelating dithiolate ligand and additional coordination from a S atom of a symmetry related CpCo(dmobdt) moiety (S1′ at $-x$, 1

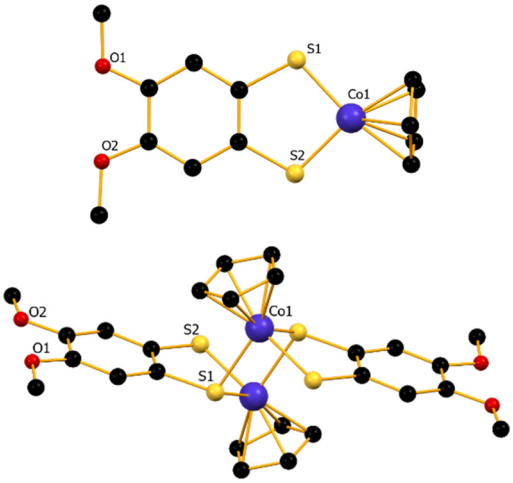

Fig. 1 Crystal structure of (top) **2a** and (bottom) **2b**. Colour code: Co^{III}, blue; S, yellow; C, black; O, red. Hydrogen atoms omitted for clarity.

$-y$, $1-z$). The Co centre is displaced from the C_6S_2Co plane of the chelating dithiolate by 0.598 Å such that the angle between the C_2S_2 and CoS_2 planes (Fig. 2) is 22.98° (*c.f.* 3.23° for **2a**). The C–S bonds in the dithiolate are 1.779(2) and 1.760(3) Å for C11–S1 and C12–S2 respectively, a little longer than in monomeric **2a**. These are intermediate between a standard C–S single bond (1.83 Å) and a thioketone (1.70 Å) and typical of other cyclopentadienyl cobalt benzenedithiolate complexes (1.75(2) Å). The Co–S bond associated with the μ_2-bridging S atoms, Co1-S2′, has a bond length of 2.2672(7) Å, similar to the monodentate Co1–S1 and Co1–S2 bond lengths (2.2309(8) and 2.2499(7) Å respectively). These Co–S bond lengths are *ca.* 0.1 Å longer than in **2a**. Isolation of both $16e^-$ monomer and $18e^-$ dimer forms has been observed in CpCo(bdt) and [CpCo(bdt)]$_2$.[21]

Complex **3**, $Cp_2Fe_2(CO)_2$(dmobdt), was crystalized from a saturated CH_2Cl_2 solution layered with hexane and adopts the triclinic space group $P\bar{1}$ with one molecule in the asymmetric unit (Fig. 2). Complex **3** comprises a CpFe(dmobdt) unit linked to a $CpFe(CO)_2$ unit with the two Fe centres bridged by a μ_2-CO ligand and one of the S atoms (S2) of the $dmobdt^{2-}$ which additionally adopts a μ_2-bridging mode. Both Fe1 and Fe2 adopt a three-legged piano stool geometry. The Fe–S bond lengths range from 2.1875(4)–2.2702(4) Å, similar to other Fe dithiolate dimers reported in the CSD (Table S4, SI), and comparable to the Co–S bond lengths in **2a** and **2b**. Comparison of the C–O distances within the two carbonyl groups reveals a longer distance of 1.178(2) Å for the bridging carbonyl compared to 1.143(2) Å for the terminal carbonyl. This is consistent with a weakened C–O bond due to greater back-donation of electron density into the π^* orbital of the CO bond from the two Fe centres. The two Cp rings are positioned in a '*cis*' conformation with a $Cp_{centroid}$–Fe–Fe–$Cp_{centroid}$ torsion angle of 2.34°. The Fe–Fe distance between the two crystallographically independent Fe centres is 2.567(3) Å. Notably, the only benzo-1,2-dithiolate complex on the CSD, structurally analogous to **3** is the parent complex $Cp_2Fe_2(CO)_2$(bdt), described by Fan and coworkers in their studies of proton reduction.[28]

Complex **4**, [CpMo(dmobdt)]$_2$, crystallizes in three separate crystal forms dependent upon crystallisation conditions: slow evaporation of **4** from dichloromethane affords the solvate-free structure **4** (Fig. 3 (top)), whereas slow evaporation from chloroform affords **4**·$CHCl_3$ (see Fig. S1, SI). Notably, attempts to prepare **4** by slow diffusion of hexanes into a saturated dichloromethane solution of **4** afforded an additional solvate, **4**·C_6H_{14} (see Fig. S1, SI)! There is negligible difference in the geometries of **4** across these three structures and the structure of the non-solvated form is discussed here. Complex **4** crystallizes in the monoclinic space group $P2_1/n$ with half a molecule in the asymmetric unit, with the two Mo centres related *via* inversion. The dimer comprises two Mo centres, each comprising four-legged piano stool geometries, bonded to one η^5-Cp ligand and four μ_2-S bridging atoms associated with the two bridging $dmobdt^{2-}$ dithiolate ligands. This coordination geometry is notably different to the cobalt complex **2b** which nominally has the same composition, [CpCo(dmobdt)]$_2$, but only

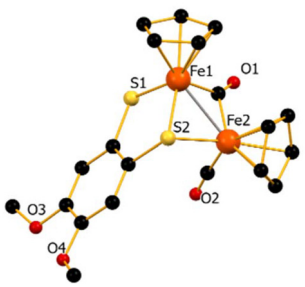

Fig. 2 Crystal Structure of **3**. Colour code: Fe^{II}, orange; S, yellow; C, black; O, red. Hydrogen atoms omitted for clarity, Fe–Fe bond represented with grey line.

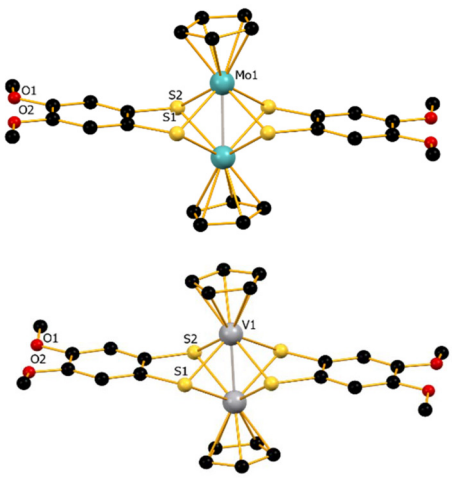

Fig. 3 Crystal structures of **4** (top) and **5** (bottom). Colour code: Mo, light blue; V, grey; S, yellow; C, black; O, red. Hydrogen atoms omitted for clarity. Close M–M contacts represented with grey line.

has two of the four S atoms adopting μ_2-bridging modes. The structure is analogous to that reported by Miller *et al.* for the related tdt^{2-} complex, $[CpMo(tdt)]_2$.[29] The Mo–S bond lengths are 2.4597(5) and 2.675(4) Å, typical for Mo-dithiolate compounds (Table S5, SI) and a little longer than those associated with the related 3d metal complexes **2** and **3**. The C–S distances (1.791(1) and 1.793(1) Å) are similar to those in the previously reported tdt^{2-} analogue as is the Mo–Mo distance of 2.5909(4) Å. The ring planes of the two crystallographically equivalent Cp groups are co planar, as are the ring planes of the two C_6S_2 groups. Conversely, the Cp and C_6S_2 rings are inclined at an angle of 11.03°.

Crystals of **5** were isolated by slow evaporation of a dichloromethane solution. Complex **5** crystalizes in the monoclinic space group $P2_1/c$ with half a molecule in the asymmetric unit. The dimeric structure is analogous to **4** (Fig. 4) with the two V centres adopting a four-legged piano stool geometry with one η^5-Cp ligand and four μ_2-S bridging atoms bonded to each metal centre. The V–S bond lengths are 2.437(1) and 2.4439(9) Å, a little longer than **2** and **3** and closer to those observed in **4** (2.4597(5) and 2.675(4) Å). A CSD search revealed six vanadium dithiolate complexes with a similar sandwich like topology,[30–33] but only one is formed with a benzenedithiolate derivative.[34] As with **4**, the C–S bond lengths in **5** (1.778(3) and 1.775(3) Å) correspond well to those in the previously published complex, as does the V–V distance of 2.5185(6) Å. Also similar to **4**, **5** comprises two sets of co-planar ring planes with respect to the Cp groups and the C_6S_2 groups, with the angle between the two sets of planes being 7.09°.

Bonding. The monomer **2a** comprises a formal Lewis acidic $16e^-$ Co(III) ion and the dithiolate S atoms are Lewis basic with each possessing 2 lone pairs. On forming the dimer, **2b**, one S atom of each dithiolate adopts a μ_2-bridging mode in which the bridging S atom donates an additional lone pair to Co such that the Co(III) ions in **2b** are each formally $18e^-$ species. Notably, the stronger donating effect of the Cp* ligand, weakens the Lewis acidity of the Co(III) centre, suppressing dimerization and all reported structures of Cp*Co(dt) complexes are monomeric in the solid state.[35–37] Previous ^{1}H solution NMR studies on CpCo(tdt) and $CpCo(S_2C_6Cl_2H_2)$ reveal a singlet for the Cp ring, indicating the presence of a single species present (either monomer or dimer), although CpCo ($S_2C_6Cl_3H$) exhibited concentration dependent ^{1}H NMR spectra which were consistent with trace amounts of dimer present at high concentration.[26,36] In the current case, **2** exhibits a singlet for the Cp ring plus singlets for the aromatic and methoxy protons. The latter two resonances are diagnostic of the monomer being present in solution, since the two S atoms (and hence the corresponding phenylene and methoxy protons) are chemically equivalent in **2a** but not in **2b**. In this context the dimeric complex $[Pt(PPh_3)(dmobdt)]_2$ shows inequivalent aromatic and methoxy peaks, indicative of the dimer being present in solution.[18] Notably the ASAP MS data (a direct insertion technique) was able to discriminate the two complexes with **2a** exhibiting an $[M + H]^+$ peak (m/z = 324.9767), whereas **2b** exhibited a $[M + H]^+$ peak at m/z = 648.9449.

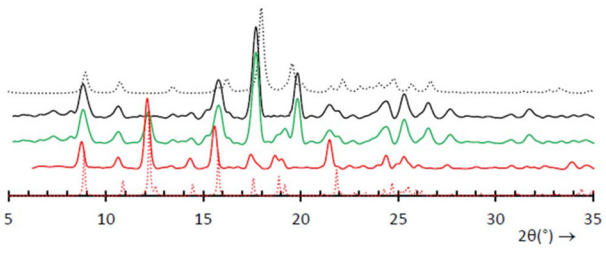

Fig. 4 PXRD patterns illustrating the effect of mechanochemical grinding on **2a**: solid black line, phase pure **2a** at room temperature; dotted black line, simulation of **2a** from SC-XRD; solid green line lightly ground sample of **2a** (resulting in a mix of **2a** and **2b**); solid red line, **2a** after sustained grinding (affording **2b**); dotted red line, simulation of **2b** from SC-XRD.

For the $Cp_2Fe_2(CO)_2(dmobdt)$ complex **3**, both Fe centres can be considered to fulfil the $18e^-$ rule provided there is an Fe–Fe bond. This is supported by the ^{1}H NMR spectrum which exhibits sharp resonances which are neither paramagnetically broadened nor paramagnetically shifted. The ^{1}H NMR of **3** exhibit two chemically distinct ^{1}H resonances (4.87 and 4.81 ppm) reflecting two chemically distinct Cp rings, similar to those in $Cp_2Fe_2(bdt)(CO)_2$ and Cp_2Fe_2 (3,6-Cl_2bdt)$(CO)_2$ recorded in d_3-MeCN.[28] The ^{1}H NMR resonances of the $dmobdt^{2-}$ ligand are consistent with a dithiolate ligand in which the two dithiolate S atoms (and hence aromatic and alkoxy protons) adopt chemically distinct environments, with two aromatic C–H and two methoxy ^{1}H resonances. These spectroscopic data for **3** are consistent with retention of the same molecular structure in both the solid state and solution. In addition, IR spectra reveal two distinct CO stretching modes at 1962 and 1749 cm^{-1}, corresponding to the terminal and μ_2-bridging CO groups. In the related complexes $Cp_2Fe_2(bdt)(CO)_2$ and $Cp_2Fe_2(3,6\text{-}Cl_2bdt)(CO)_2$, the terminal CO stretching vibration occurs notably higher in energy (1987 and 1992 cm^{-1} respectively), reflecting the stronger donor nature of the $dmobdt^{2-}$ ligand. Similarly, the bridging μ-CO in both $Cp_2Fe_2(bdt)(CO)_2$ and $Cp_2Fe_2(3,6\text{-}Cl_2bdt)(CO)_2$ also occur higher in frequency (1804 and 1811 cm^{-1} respectively) than **3**. Notably complexes **2**, **4** and **5** all reveal complete elimination of CO during oxidative addition of **1** to the $CpM(CO)_n$ precursor but **3** does not. Elimination of two equivalents of CO from **3** would afford $Cp_2Fe_2(dmobdt)$. Structures of this type are formally $16e^-$ compounds and have been reported for several complexes with strong donor cyclopentadienyl groups including $Cp^*_2Fe_2(bdt)$ and $Cp^*_2Fe_2(dmobdt)$.[38,39] In the case of **3** there was no evidence for formation of $Cp_2Fe_2(dmobdt)$ within the reaction mixture. In this regard, photolysis of $[CpFe(CO)_2]_2$ with one equivalent of $bdtH_2$ forms $Cp_2Fe_2(CO)_2(bdt)$ (analogous to **3**), whereas photolysis of $[CpFe(CO)_2]_2$ with two equivalents of $bdtH_2$ formed the dimer $[CpFe(bdt)]_2$, structurally similar to **2b**.[28] In this work attempts to form $[CpFe(dmobdt)]_2$, compositionally analogous to **2b**, **4** and **5** *via* stoichiometric control were unsuccessful: reaction of $[CpFe(CO)_2]_2$

with both 0.5 or 1.0 equivalent of **1** afforded only the mono-dithiolate complex **3**.

For complex **4**, the compound is formally $17e^-$, or $18e^-$ if a Mo–Mo bond is present. This complex is structurally similar to the dimers $[CpMo(bdt)]_2$ and $[CpMo(tdt)]_2$.[29] The sharpness of the ^{1}H NMR spectrum and the observed chemical shift range are indicative of a diamagnetic complex, supporting the hypothesis of a formal Mo–Mo bond. Conversely for complex **5**, the vanadium centre is formally $16e^-$, or $18e^-$ for a V=V double bond. Previous work has described the synthesis of three other [V_2-dithiolate] compounds: $[V_2(edt)_4]$ is described as containing either a V–V single or double bond based upon crystallographic data, the diamagnetic nature of the compound and MO calculations.[31,32] On the other hand, $[Cp_2V_2(S_2)(S_2C_4F_6)]$ is weakly paramagnetic.[33] Work by Stephan described the synthesis of the analogous dimer, $[CpV(bdt)]_2$ but did not report any NMR data.[34]

In this work NMR data was similarly difficult to obtain with standard ^{1}H NMR procedures not affording an interpretable spectrum, suggesting **5** retains its paramagnetic nature as described by Stephan, leading to significant line broadening, peak shifting and reduced signal intensities.[34]

Phase behaviour of 2. Derivatives of CpCo(bdt) have been found to adopt either monomeric $16e^-$ or $18e^-$ dimeric structures (eqn (1)):[40]

$$[CpCo(bdt)]_2 \rightleftharpoons 2\ CpCo(bdt) \quad (1)$$

Formation of dimers is enthalpically favoured through formation of two S → Co dative covalent bonds, whereas the monomeric $16e^-$ complexes are entropically favoured. Nomura *et al.* showed from dilute solution UV/vis studies that the entropically favoured monomer phase dominates in solution.[26] Nevertheless, at high concentration, ^{1}H NMR studies reflected the presence of the dimer form as the minor component (monomer : dimer ~ 40 : 1 for $CpCo(S_2C_6Cl_4)$). The related selenium analogue, $[CpCo(Se_2C_6H_4)]_2$, appears more stable in the dimer form and reveal $\Delta H_{dim} = -60$ kJ mol^{-1} in d^6-benzene and $\Delta S_{dim} = -120$ J K^{-1} mol^{-1}. Dimer formation is favored by (i) enhancing the Lewis basicity of the dithiolate S atoms and (ii) increasing the Lewis acidity of the cobalt(III) centre. In this regard, the strongly donor Cp* ligand reduces the Lewis acidity of Co(III) and crystal structures of Cp*Co(bdt) derivatives are all monomeric in the solid state. Conversely, crystal structures of CpCo(bdt) derivatives are reported to be variously monomers or dimers in the solid state, indicating a subtle balance between monomer and dimer forms. Among these derivatives, CpCo(bdt) (**6**) has previously appeared unique in forming both monomer (**6a**) and dimer (**6b**) phases. Slow crystallization was reported to favour **6b** (enthalpic product) whereas sublimation or rapid crystallization favors **6a** as the entropic product. For **6**, the two phases were reported to interconvert in the solid state with the dimerization process **6a**(s) → **6b**(s) occurring slowly at room temperature and the reverse process, **6b**(s) → **6a**(s) occurring at 150 °C. DSC studies revealed $\Delta H_{rxn} = +18.9$ kJ mol^{-1} for the process **6b**(s) → **6a**(s) at 150–160 °C.

In the current study, we similarly found that monomeric **2a** is isolated by sublimation at elevated temperatures, whereas crystal growth from solution at room temperature forms dimeric **2b**. Room temperature powder X-ray diffraction (PXRD) studies on unground samples confirmed the phase purity of monomeric **2a** and dimeric **2b** phases, by comparison with simulated PXRD profiles based on low temperature single crystal structure determinations (Fig. S2 and S3, SI). Although the two PXRD profiles share certain similarities, **2a** and **2b** could be readily distinguished on the basis of two reflections: the (0 1 1) reflection present in **2b** at $2\theta \sim 12°$ and the (2 0 0) reflection at $2\theta \sim 20°$ associated with **2a** (Fig. 4). Variable temperature PXRD measurements on **2b** (Fig. S4, SI) show no change in the PXRD profile between room temperature and 150 °C (the upper limit of our measurements).

DSC studies reveal that **2a** melts at 206 °C and **2b** melts at 216 °C (Fig. S7, SI). The enthalpies of fusion are $\Delta_{fus}H$ = +21.9 kJ mol^{-1} for **2a** and $\Delta_{fus}H$ = +51.9 kJ mol^{-1} for **2b**. This provides an approximate $\Delta_{dim}H$ [2 × **2a**(s) → **2b**(s)] of −8.1 kJ mol^{-1}. This is comparable with that observed for the process 2 × **6a**(s) → **6b**(s) at −18.9 kJ mol^{-1}. After cooling **2b** from the melt (−10 K min^{-1}) and stabilizing at 25 °C for 5 minutes, a re-heat cycle (+10 K min^{-1}) revealed the emergence of a feature at 206 °C diagnostic of **2a** in addition to the expected melting of **2b** at 216 °C (Fig. S8, SI). This indicated that melting affords a mixture of **2a** and **2b**.

Although there was no evidence for a solid-state phase transition from **2a**(s) to **2b**(s) upon standing, nor conversion from **2b**(s) to **2a**(s) upon heating, we were intrigued by initial PXRD measurements: our PXRD samples are typically lightly ground prior to measurement to minimize preferred orientation effects and a sample of **2a** subjected to brief grinding afforded a PXRD pattern reflecting the presence of both **2a** and **2b**. Optical examination of the remaining pristine sample suggested that **2a** was homogeneous, suggesting a mechanochemical transformation from **2a** to **2b** (Fig. 4). Upon prolonged grinding, complete conversion of **2a** into **2b** was achieved (Fig. 4). Attempts to convert dimer **2b** into monomeric **2a** upon grinding were unsuccessful revealing dimerization is an irreversible process at ambient temperature. This led us to contemplate the different solid state behaviours of **2** and **6**.

As pointed out by West, solid-state reactions can only occur if reactive centres are in the right orientation and sufficiently close together.[41] This suggests that molecular displacements in solid state reactions are typically short. Miller's study on **6** revealed that monomer **6a** has two molecules in the asymmetric unit. Each crystallographically independent molecule forms a pair of close, intermolecular Co···S contacts (Co1···S1 at 4.703 Å and Co2···S3 at 5.060 Å) linking molecules related *via* inversion symmetry (Fig. 5a). In both cases, shortening these contacts generates a centrosymmetric dimer with Co–S bonds of 2.272 Å (Fig. 5b). In the case of **2a**, there is a single molecule in the asymmetric unit. This molecule exhibits a close intermolecular Co···S contact (4.719 Å, Fig. 5c) similar to that observed in **6a** but this pair of molecules is not related *via*

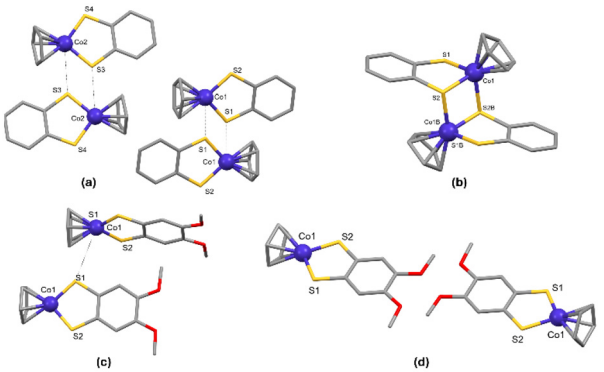

Fig. 5 (top) Comparison of the molecular displacements with respect to inversion in (a) the monomer **6a**, (b) the dimer **6b**; (bottom): (c) the closest Co···S contact between monomers in **2a** and (d) monomers related *via* inversion symmetry in **2a**.

a crystallographic inversion centre. Instead, these close Co···S contacts in **2a** are related *via* a glide plane and are therefore not of the correct orientation to undergo centrosymmetric dimerization. The space group *Pbca* observed for complex **2a** does exhibit a crystallographic inversion centre, but molecules related by inversion exhibit long Co···S separations at 12.747 and 13.735 Å (Fig. 5d). These are well beyond the short molecular displacements typically associated with solid state transformations and are consistent with the lack of thermal interconversion between **2a** and **2b** in the solid state. The mechanochemically-driven transition from **2a** to **2b**, presumably displaces monomers with respect to the inversion. A comparison of the unit cells of **2a** and **2b** (Table S1, SI) indicate that the two structures are related *via* a doubling of the crystallographic *c*-axis. The packing of **2a** and **2b** in the *bc* plane (Fig. 6) highlights the similarity in the two structures. While the transformation from **2a** to **2b** is thermodynamically favoured based on (i) the density rule,[42] and (ii) the estimated difference in $\Delta_{fus}H$, there is likely a large activation barrier to this structural transformation. This is not achieved thermally up to the melting point but is seemingly driven mechanochemically at ambient temperature. Recent studies have highlighted the importance of mechanical stress reducing the reaction energy barrier for shear-driven transformations.[43] Similar investigations on dimeric complexes **4** and **5** revealed no evidence for similar phase transitions, likely due to the instability of the $12e^-$ CpV(dmobdt) and $13e^-$ CpMo(dmobdt) monomers in relation to $16e^-$ CpCo(dmobdt).

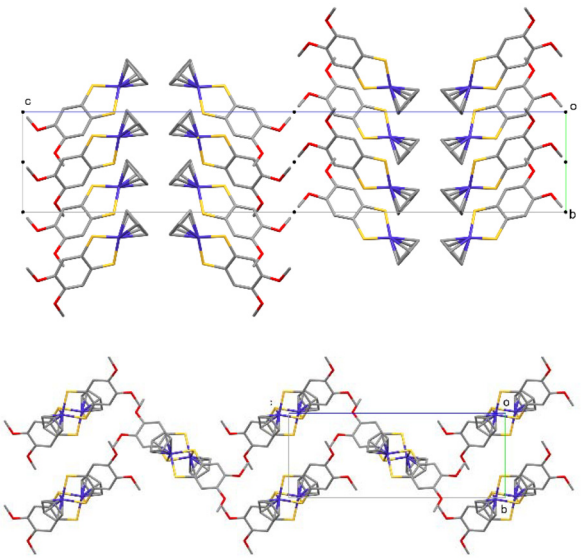

Fig. 6 (top) Molecular packing of **2a** viewed along the crystallographic *a*-axis, highlighting inversion centres (•); (bottom) molecular packing of **2b**, also viewed along the crystallographic *a*-axis. [H atoms omitted for clarity].

Conclusions

In summary, the current study expands the synthetic methodology of microwave-assisted oxidative addition reactions of tetrathiocins, such as **1**, as a route to transition metal dithiolate complexes for a variety of early, mid and late transition metals from the 3d and 4d series. In the current study oxidative addition of **1** to half-sandwich cyclopentadienyl metal carbonyl complexes occurs with partial or complete elimination of CO. In particular, the cobalt complexes **2a** and **2b** form distinct monomeric and dimeric structures with the entropically favored monomer formed by sublimation at high temperature and the dimer form afforded by recrystallization at room temperature. Heating the dimer into the melt phase generates some monomer based on DSC measurements, whereas mechanochemical grinding of **2a** affords **2b** *via* an irreversible mechanochemical phase transition.

Conflicts of interest

There are no conflicts to declare.

Data availability

A summary of analytical data and instrumentation used for elemental analysis, IR, MS, NMR; plots of PXRD and DSC data are freely available and summarized in the experimental section of the SI. See DOI: https://doi.org/10.1039/d5dt01691f.

CCDC 2470686–2470691 and 2471388 (**2a**, **2b**, **3**, **4**, **4**·$CHCl_3$, **4**.C_6H_{12} and **5**) contain the supplementary crystallographic data for this paper.[44(a–g)] The crystallographic data supporting this article have also been included as part of the SI.

Acknowledgements

The work was supported through NSERC DG (J. M. R. DG 2020-04627; M. P. DG-2018-0425/2024-04043; C. L. B. M. DG 2024-04186), NSERC RTI (J. M. R. RTI-2022-00005; M. P. RTI-2020-00310) and CFI/ORF award (LOF-212442). DJC thanks the European Union's Horizon 2020 research and innovation programme under the Marie Skłodowska-Curie grant (#101151188).

References

1 (*a*) J. A. McCleverty and T. J. Meyer, *Comprehensive Coordination Chemistry II: From Biology to Nanotechnology*, Newnes, 2003; (*b*) R. Eisenberg and H. B. Gray, *Inorg. Chem.*, 2011, **50**, 9741–9751.

2 S. D. Cummings, L. T. Cheng and R. Eisenberg, *Chem. Mater.*, 1997, **9**, 440–450.

3 L. Pilia, D. Marinotto, M. Pizzotti, F. Tessore and N. Robertson, *J. Phys. Chem. C*, 2016, **120**, 19286–19294.

4 (*a*) G. Li, M. F. Mark, H. Lv, D. W. McCamant and R. Eisenberg, *J. Am. Chem. Soc.*, 2018, **140**, 2575–2586; (*b*) A. Singh, P. Singh, G. Kociok-Köhn, M. Trivedi, A. Kumar, R. Chauhan, S. B. Rane, C. Terashima, S. W. Gosavi and A. Fujishima, *New J. Chem.*, 2018, **42**, 9306–9316.

5 M. Yamashita, Y. Sato, Y. Kasahara, S. Kasahara, T. Shibauchi and Y. Matsuda, *Sci. Rep.*, 2022, **12**, 9187.

6 K. Takada, M. Ito, N. Fukui and H. Nishihara, *Commun. Chem.*, 2024, **7**, 186.

7 M. Tran, Y. Wang, B. Dzikovski, M. E. Lahm, Y. Xie, P. Wei, V. V. Klepov, H. F. Schaefer and G. H. Robinson, *J. Am. Chem. Soc.*, 2024, **146**, 16340–16347.

8 F. Santanni, M. Briganti, G. Serrano, E. Salvadori, A. Veneri, C. Batistoni, S. F. Russi, S. Menichetti, M. Mannini, M. Chiesa, L. Sorace and R. Sessoli, *JACS Au*, 2023, **3**, 1250–1262.

9 (*a*) K. Koshiba, K. Yamauchi and K. Sakai, *Angew. Chem., Int. Ed.*, 2017, **56**, 4247–4251; (*b*) Z. Liu, C. Xu, J. del Pozo, S. Torker and A. H. Hoveyda, *J. Am. Chem. Soc.*, 2019, **141**, 7137–7146.

10 J. A. Denny and M. Y. Darensbourg, *Chem. Rev.*, 2015, **115**, 5248–5273.

11 H. Alves, D. Simão, I. C. Santos, V. Gama, R. T. Henriques, H. Novais and M. Almeida, *Eur. J. Inorg. Chem.*, 2004, **2004**, 1318–1329.

12 L. K. Watanabe, Z. S. Ahmed, J. J. Hayward, E. Heyer, C. L. B. Macdonald and J. M. Rawson, *Organometallics*, 2022, **41**, 226–234.

13 L. K. Watanabe, J. D. Wrixon and J. M. Rawson, *Dalton Trans.*, 2021, **50**, 13620–13633.

14 Y. Nakamura, T. Matsumoto, Y. Sakazume, J. Murata and H. C. Chang, *Chem. – Eur. J.*, 2018, **24**, 7398–7409.

15 E. J. Wharton and J. A. McCleverty, *J. Chem. Soc. A*, 1969, 2258–2266.

16 J. D. Wrixon, J. J. Hayward and J. M. Rawson, *Inorg. Chem.*, 2015, **54**, 9384–9386.

17 L. K. Watanabe, J. D. Wrixon, Z. S. Ahmed, J. J. Hayward, P. Abbasi, M. Pilkington, C. L. B. MacDonald and J. M. Rawson, *Dalton Trans.*, 2020, **49**, 9086–9093.

18 J. D. Wrixon, Z. S. Ahmed, M. U. Anwar, Y. Beldjoudi, N. Hamidouche, J. J. Hayward and J. M. Rawson, *Polyhedron*, 2016, **108**, 115–121.

19 J. D. Wrixon, J. J. Hayward, O. Raza and J. M. Rawson, *Dalton Trans.*, 2013, **43**, 2134–2139.

20 G. B. Jameson, H. R. Oswald and H. R. Beer, *J. Am. Chem. Soc.*, 1984, **106**, 1669–1675.

21 E. J. Miller, T. B. Brill, A. L. Rheingold and W. C. Fultz, *J. Am. Chem. Soc.*, 1983, **105**, 7580–7584.

22 K. W. Stender, N. Wolki and G. Klar, *Phosphorus, Sulfur Silicon Relat. Elem.*, 1989, **42**, 111–114.

23 A. Alberola, D. Eisler, R. J. Less, E. Navarro-Moratalla and J. M. Rawson, *Chem. Commun.*, 2010, **46**, 6114–6116.

24 S. Tsukada, M. Kondo, H. Sato and T. Gunji, *Polyhedron*, 2016, **117**, 265–272.

25 M. Nomura, E. Tsukano, C. Fujita-Takayama, T. Sugiyama and M. Kajitani, *J. Organomet. Chem.*, 2009, **694**, 3116–3124.

26 M. Nomura, T. Sasao, T. Hashimoto, T. Sugiyama and M. Kajitani, *Inorg. Chim. Acta*, 2010, **363**, 3647–3653.

27 M. Nomura and M. Fourmigué, *J. Organomet. Chem.*, 2007, **692**, 2491–2499.

28 W. L. J. Loke and W. Y. Fan, *Int. J. Hydrogen Energy*, 2020, **45**, 31976–31984.

29 W. K. Miller, R. C. Haltiwanger, M. C. Vanderveer and M. R. Dubois, *Inorg. Chem.*, 1983, **22**, 2973–2979.

30 O. A. Rajan, M. McKenna, J. Noordik, R. C. Haltiwanger and M. R. DuBois, *Organometallics*, 1984, **3**, 831–840.

31 D. Szeymies, B. Krebs and G. Henkel, *Angew. Chem., Int. Ed. Engl.*, 1983, **22**, 885–886.

32 J. R. Dorfman and R. H. Holm, *Inorg. Chem.*, 1983, **22**, 3179–3181.

33 C. M. Bolinger, T. B. Rauchfuss and A. L. Rheingold, *J. Am. Chem. Soc.*, 1983, **105**, 6321–6323.

34 D. W. Stephan, *Inorg. Chem.*, 1992, **31**, 4218–4223.

35 M. Nomura, E. Tsukano, C. Fujita-Takayama, T. Sugiyama and M. Kajitani, *J. Organomet. Chem.*, 2009, **694**, 3116–3124.

36 S. Tsukada, M. Kondo, H. Sato and T. Gunji, *Polyhedron*, 2016, **117**, 265–272.

37 M. Nomura and M. Fourmigué, *Inorg. Chem.*, 2008, **47**, 1301–1312.

38 D. Yang, Y. Li, B. Wang, X. Zhao, L. Su, S. Chen, P. Tong, Y. Luo and J. Qu, *Inorg. Chem.*, 2015, **54**, 10243–10249.

39 T. Sun, S. Xu, D. Yang, L. Su, B. Wang and J. Qu, *Eur. J. Inorg. Chem.*, 2020, **2020**, 4263–4269.

40 M. Nomura, *Dalton Trans.*, 2011, **40**, 2112–2140.

41 A. R. West, *Solid State Chemistry and its Applications*, J. Wiley and Sons, Chichester, UK, 1984.

42 A. Burger and R. Ramberger, *Microchim. Acta*, 1979, **72**, 273–316.

43 F. H. Bhuiyan, Y.-S. Li, S. H. Kim and A. Martini, *Sci. Rep.*, 2024, **14**, 2992.

44 (*a*) CCDC 2470686: Experimental Crystal Structure Determination, DOI: 10.5517/ccdc.csd.cc2nxyk3; (*b*) CCDC 2470687: Experimental Crystal Structure Determination, DOI: 10.5517/ccdc.csd.cc2nxyl4; (*c*) CCDC 2470688: Experimental Crystal Structure Determination, DOI: 10.5517/ccdc.csd.cc2nxym5; (*d*) CCDC 2470689: Experimental Crystal Structure Determination, DOI: 10.5517/ccdc.csd.cc2nxyn6; (*e*) CCDC 2470690: Experimental Crystal Structure Determination, DOI: 10.5517/ccdc.csd.cc2nxyp7; (*f*) CCDC 2470691: Experimental Crystal Structure Determination, DOI: 10.5517/ccdc.csd.cc2nxyq8; (*g*) CCDC 2471388: Experimental Crystal Structure Determination, DOI: 10.5517/ccdc.csd.cc2nyp6j.